

Synchronizing Bloch-oscillating free carriers in moiré flat bands

Ali Fahimniya¹, Zhiyu Dong¹, Egor Kiselev², Leonid Levitov¹

¹*Physics Department, Massachusetts Institute of Technology, Cambridge, Massachusetts 02139, USA*

²*Institut für Theorie der Kondensierten Materie,
Karlsruher Institut für Technologie, 76131 Karlsruhe, Germany*

Bloch oscillations of free charge carriers in narrow-band superlattices, arising under an applied direct current, is a striking collective many-body behavior with possible applications for converting a direct current into a high-frequency current in THz domain. We argue that the flat bands in recently introduced moiré superlattices fulfill the basic requirements for observing Bloch oscillations. These two-dimensional superlattices provide an appealing alternative to the quasi-1D semiconducting superlattice arrays in which previous work aiming to achieve collective Bloch oscillations was carried out. The asynchronous free-carrier oscillations can be synchronized through coupling to an oscillator mode, realized as a THz photonic or plasmonic resonator. We present a detailed analysis of the phase diagram of the system that shows a transition between the asynchronous regime and a synchronized phase-coherent collective oscillation regime.

Bloch oscillations, arising when electrons are driven through a perfect crystal lattice by an electric field, is an iconic example of a coherent dynamics in an externally driven quantum many-body system[1, 2]. The oscillation frequency is determined solely by lattice periodicity a and field strength E , so that all carriers oscillate at the same frequency, for a one-dimensional lattice given by $f = eEa/h$. This behavior points to an appealing possibility to convert a DC current into a high-frequency AC current[3]. Besides the obvious fundamental appeal, wide interest in this phenomenon also stems from the expectation that Bloch oscillating electrons have the potential to provide broad band gain at THz frequencies[4, 5] and become the basis of a technology that will help fill the gap in solid state THz fundamental oscillators, leading to radiation emitters and detectors operating in the THz frequency range[6].

While Bloch oscillations have long been immortalized in textbooks, realizing them in solids has proven to be a challenging task due to fairly stringent requirements on the system. Achieving this regime requires overcoming several obstacles. One the electron energy loss due to phonon emission that dephases the oscillations. To suppress phonon emission exceptionally narrow electronic bands of width much smaller than the optical phonon energy must be used. Another is the dephasing due to disorder scattering. The experimental efforts so far mainly focused on synthetic MBE-grown semiconductor superlattices, which host Bloch minibands of narrow width tunable by the superlattice design parameters[6–9]. The superlattice systems cleared a number of key milestones on the road towards achieving Bloch oscillations. Namely, they display the signatures indicative of Bloch oscillations, such as negative differential conductivity $dI/dV < 0$, recurrence and ringing in the optical pump-probe measurements, Wannier-Stark ladders and optical gain[6–9]. However, upon the DC current increasing and approaching the relevant parameter range the superlattice systems develop instabilities and show a complex noisy behavior due to the onset of switching and formation of electric domains. This behavior presents

the main obstacle to achieving the collective globally-synchronized Bloch oscillations[11–13].

Meanwhile, recently Bloch oscillations were achieved in cold atom systems, using Bloch minibands in optical lattices[14–18]. Because the systems is charge-neutral, instead of the electric field the force of gravity had to be used to accelerate particles. This proof-of-principle demonstration has greatly improved our understanding of the underlying physics[19, 22] and strengthened interest in demonstrating electronic Bloch oscillations.

Given the difficulties encountered in semiconducting superlattices it is natural to look for other systems that meet the requirements for achieving Bloch oscillations, but are not prone to the electric domain formation instabilities. One enticing opportunity is offered by the recently introduced moiré superlattices in twisted bilayer graphene, a material that hosts electron bands that are tunable by the twist angle[23–28]. For twist angles $\theta \lesssim 2^\circ$ the moiré electron bands are considerably narrower than the optical phonon energy (~ 200 meV), becoming as narrow as $J \lesssim 10\text{--}20$ meV near “magic” values of the twist angle $\theta \sim 1^\circ$. Such bandwidths are sufficient to eliminate the optical phonon emission, the main obstacle to observing coherent Bloch oscillations in wide bands.

The moiré graphene also clears other key requirements for observing Bloch oscillations. One is weak disorder scattering. Since the narrow bands are formed in a solid with a pristine near-perfect atomic order, they are less susceptible to disorder than the bands in synthetic MBE-grown semiconductor superlattices. This is manifested in a high carrier mobility and ballistic carrier transport observed over micron lengthscales at $T = 0$ [27, 28]. Estimating the scattering time as $\tau = l/v_F$ with the mean free path $l \sim 1 \mu\text{m}$ and v_F of about 1/30 of the graphene monolayer value 10^6 m/s gives $\tau \sim 3 \cdot 10^{-11}$ s, a value comparable to that of graphene monolayer. The scattering rate therefore can be two orders of magnitude smaller than the bandwidth, $\gamma_{\text{dis}} \sim 10^{-2} J$.

Furthermore, the two-dimensional character of moiré graphene will help to suppress the instability due to inhomogeneous charge accumulation that drives the for-

mation of electric field domains occurring in the stacks of quantum wells. Indeed, in the moiré setup the electric current is driven in the graphene plane in a manner that maintains the translation invariance of the system and does not cause local charging. In addition, gating is known to maintain a spatially uniform carrier density even under moderate to high currents.

Other appealing properties of moiré graphene are the lack of Zener transitions, suppressed by sizable minigaps separating the flat bands from other minibands, and the weakness of the electron-phonon scattering by the long-wavelength acoustic phonons[29–31]. Added to that, the relatively large periodicity of moiré superlattices ($a \sim 10\text{nm}$) reduces the required E field values:

$$\gamma = \max[\gamma_{\text{ph}}, \gamma_{\text{dis}}] < \omega_B < J/\hbar, \quad \omega_B = eEa/\hbar. \quad (1)$$

Using moderate E fields will help to avoid the Wannier-Stark ladder localization effects and charge instabilities.

Importantly, although all free carriers Bloch oscillate with identical frequencies, these oscillations are *asynchronous*, as the oscillation phases are totally random and uncorrelated for different carriers. Therefore, in order to achieve collective continuous-wave Bloch oscillations driven by a direct current, the movement of different carrier must be synchronized. We demonstrate that this can be achieved through coupling of the current-carrying channel to an oscillator mode in a THz resonator. The frequency of the resonator depends on system parameters, at the same time the Bloch frequency is tunable by varying the applied DC electric field. As we will see, this system exhibits an instability towards collective oscillations at a Bloch frequency when the latter is close to the oscillator frequency. In practice, the oscillator can be realized as a THz photonic or plasmonic resonator in a 2D or a 3D architecture[6, 32–36]. The phase diagram of the system shows the asynchronous regime and several interesting synchronized collective oscillation regimes.

Prior to presenting the analysis of the synchronization problem we summarize the basic picture of the asynchronous free-carrier Bloch oscillations in superlattices. The dynamics in superlattices of dimension $D \geq 2$ differs from that in $D = 1$ in that different carriers can move at different angles relative to the applied field[10, 19–22]. Despite this difference, the main properties of the one-dimensional Bloch oscillations persist. The Bloch frequencies remain discrete, taking values identical for all carriers in the system. The only new aspect is that different harmonics of the band dispersion produce oscillations with several different discrete frequency values. These frequencies are in general incommensurate with one another. The frequency values can be adjusted by changing the field orientation, as illustrated in Fig.1.

The frequency values have a peculiar dependence on the electric field orientation with respect to the superlattice axes, described by the geometric construction illustrated in Fig.1. Namely, possible frequencies are given by the projections of different Bravais lattice vectors

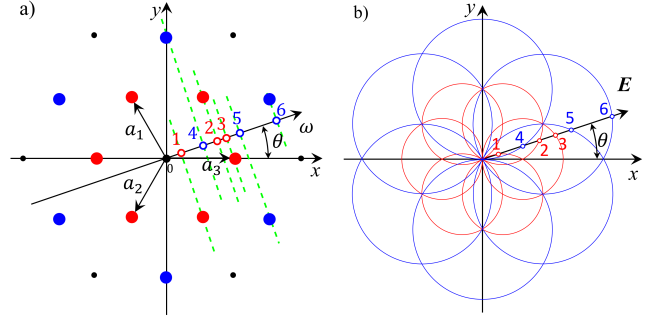


FIG. 1: a) A depiction of the method to determine the discrete Bloch oscillation frequency values ω in a superlattice for a generic electric field orientation. Illustrated is the geometric construction in Eq.(2) in a 2D solid with trigonal symmetry. The real-space Bravais lattice points (solid circles), are projected onto the 1D line parallel to \mathbf{E} (black arrow) as indicated by dashed green lines. The shortest and next-shortest vectors are shown as red and blue dots. Hollow circles, found by projection, give the frequencies in Eq.(2), where the emitted noise power $P(\omega)$ peaks. b) Visualization of the Bloch frequencies angle dependence vs. \mathbf{E} orientation.

$\mathbf{a}_l = n_1 \mathbf{a}_1^{(0)} + n_2 \mathbf{a}_2^{(0)}$ on the applied field \mathbf{E} :

$$\omega_l = \frac{e}{\hbar} \mathbf{E} \cdot \mathbf{a}_l = \frac{e}{\hbar} E a_l \cos(\theta - \theta_l) \quad (2)$$

The dependence of the frequencies ω_l on the field \mathbf{E} orientation and strength, as well as the tunability of moiré superlattices by the twist angle, provide knobs that will facilitate achieving Bloch oscillations in moiré graphene.

This result can be understood by considering a generic tight binding bandstructure on a monoatomic lattice,

$$\epsilon(\mathbf{k}) = \sum_{l=1,2,\dots} -2J_l \cos(\mathbf{k} \cdot \mathbf{a}_l), \quad (3)$$

where \mathbf{a}_l are vectors in the Bravais lattice, describing hopping between different pairs of lattice sites. Bloch oscillating free carriers obey quasiclassical equations of motion

$$\hbar \frac{d\mathbf{k}}{dt} = e\mathbf{E}, \quad (4)$$

generating a linear time dependence $\mathbf{k}(t) = \frac{e}{\hbar} \mathbf{E}t + \mathbf{k}_0$ with the linear part identical for all carriers and a carrier-specific initial value \mathbf{k}_0 . With this bandstructure and an electric field of a general orientation, $\mathbf{E} = E(\cos \theta, \sin \theta)$, the frequencies at which the time-dependent velocity of the electrons $\mathbf{v} = \frac{1}{\hbar} \nabla_{\mathbf{k}} \epsilon(\mathbf{k})$ will oscillate are given by \mathbf{a}_l projected on \mathbf{E} , Eq.(2). The resulting dependence of the frequencies ω_l on the orientation of \mathbf{E} is described by families of circles pictured in Fig.1.

Physically, discrete frequency values arise because electron trajectories sweep the (reduced) Brillouin zone (BZ) of a two-dimensional crystal in the direction set by the \mathbf{E} vector. Every time an electron reaches zone boundary it umklapps to the opposite side and continues forward, winding around the BZ at different frequencies in

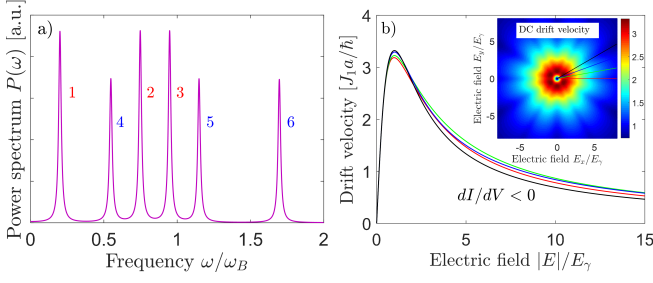


FIG. 2: Testable signatures of asynchronous (free-carrier) Bloch oscillations. a) Ensemble-averaged AC current power spectrum, Eqs.(5), features finite-width resonances at the discrete frequency values ω_l , Eq.(2); units: $\omega_B = \frac{e}{\hbar} E a$. The red and blue labeling of different peaks and the field orientation used match those in Fig.1. b) The DC drift velocity, Eq.(6). Shown is the full dependence (inset) and traces for several different field orientations. Bloch oscillations occur for field strength $E > E_\gamma = \hbar\gamma/ea$; negative differential DC conductivity $dI/dV < 0$ is a hallmark of this regime.

different crystal axes directions. At the same time, the average frequency along the direction of \mathbf{E} is the same for all carriers. This leads, for a general field orientation, to a quasiperiodic dynamics characterized by two fundamental frequencies which depend only on the field \mathbf{E} and lattice periodicity as described in Eq.(2), wherein $\omega_l = n_1\omega_1 + n_2\omega_2$ in agreement with the geometric construction in Fig.1.

In the presence of momentum-relaxing scattering the frequency spectrum broadens into a sum of finite-width resonances centered at $\omega = \omega_l$. The emitted power spectrum is proportional to the autocorrelation function of current fluctuations, given by a sum of Lorentzians:

$$P(\omega) = \frac{1}{2} \int_{-\infty}^{\infty} \langle \delta \mathbf{j}(t) \cdot \delta \mathbf{j}(t + \tau) \rangle e^{-i\omega\tau} d\tau$$

$$= \sum_l \frac{P_l}{(\omega - \omega_l)^2 + \gamma^2}, \quad (5)$$

where $\langle \dots \rangle$ denotes ensemble averaging (see Appendix for derivation and the discussion of the validity of this result). Since the frequencies ω_l are proportional to the applied field \mathbf{E} the oscillations appear when the field strength exceeds a threshold set by momentum-relaxing scattering, $E_\gamma = \hbar\gamma/ea$. At lower fields different resonances merge into a broadband noise spectrum, indicating a suppression of the oscillations.

In the Bloch oscillation regime the DC drift velocity exhibits negative differential conductivity $dI/dV < 0$, a characteristic behavior that provides a clear signature of this regime. A simple model (see Appendix) predicts

$$\mathbf{j}_{\text{DC}} = \frac{e}{\hbar} \sum_l l J_l f_{0,l} \frac{\gamma \omega_l}{\gamma^2 + \omega_l^2} \quad (6)$$

featuring a dependence on the driving field which is linear at small $E < E_\gamma$ and falls off as $1/E$ at large $E > E_\gamma$. In-

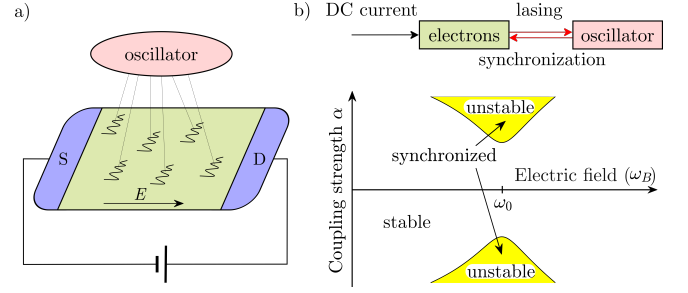


FIG. 3: a) Schematic of Bloch oscillating electrons synchronized by coupling to an oscillator mode. An electric field \mathbf{E} due to voltage source drives free-carrier oscillations with frequency ω_B (wavy lines). The free-carrier oscillations are at the same frequency for all carriers but are asynchronous (not in phase). The couplings between the electrons and the oscillator mode, depicted by the thin lines, can synchronize the oscillations. b) A phase diagram showing the stable and unstable regimes, in which Bloch oscillations are asynchronous and synchronized, respectively. The carrier scattering rate γ is taken to be equal the oscillator damping rate γ_0 (see Eq.(17)); phase diagrams for unequal γ and γ_0 are pictured in Fig.4. The Bloch frequency ω_B on the x axis is proportional to the electric field; ω_0 is the oscillator frequency, the coupling strength α between each electron and the oscillator is defined in Eq.(10). Instability is easiest to achieve when ω_B is tuned close to ω_0 . The flowchart on top shows the relationship between the electrons in the system and the oscillator mode in the unstable phase. The DC drives free-carrier oscillations, the oscillations are synchronized by the oscillator and, in turn, pump energy into the oscillator (the lasing effect).

terestingly, current depends on the dimensionless quantity E/E_γ in a way that is independent of the specific value of γ . This behavior is illustrated in Fig.2(b). The drift velocity for electric fields in different directions is shown in the inset.

Next, we turn to the discussion of Bloch oscillations synchronized by coupling to an oscillator mode, realized as e.g. THz photonic or plasmonic resonators[6, 32–36]. We consider the near-resonant case when the oscillator frequency is close to one of the free-carrier harmonics given in Eq.(2). It is therefore sufficient to focus on the one-frequency Bloch oscillations described by the Hamiltonian

$$H = \sum_i [\epsilon(p_i) - eEx_i - \alpha Qx_i] + \frac{1}{2m} P^2 + \frac{\omega_0^2 m}{2} Q^2. \quad (7)$$

Here $\epsilon(p)$ is the band dispersion, p_i and x_i are the momenta and coordinates of the electrons; P and Q are the momentum and amplitude of the oscillator. The Bloch electron coupling to the oscillator and the external field is through potentials $U(x_i) = -eEx_i - \alpha Qx_i$ seen by each of the electrons.

In this approach we ignore the carrier-carrier interactions, treating electron dynamics in a free-particle approximation. Bloch oscillations are driven by the electric field E , the term $-\alpha Qx_i$ describes coupling of the electrons to the oscillator mode. For conciseness, we present

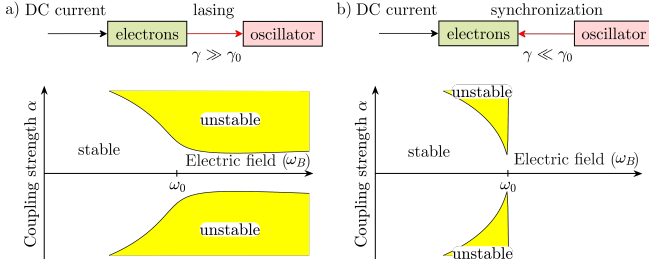


FIG. 4: The lasing and synchronization regimes. a) Lasing ($\gamma \gg \gamma_0$). In this case, the oscillator is under-damped and serves as the main reservoir of the energy. Energy of the electrons is more easily pumped to the oscillator when $\omega_B > \omega_0$. Shown is the phase diagram for $\gamma = 100\gamma_0$. b) Synchronization ($\gamma \ll \gamma_0$). In this case, the oscillator is over-damped and the electrons serve as the main reservoir of the energy. Energy of the oscillator is more easily pumped to the electrons when $\omega_B < \omega_0$. Shown is the phase diagram for $100\gamma = \gamma_0$. The instability criterion is a sign change of the imaginary parts of the roots of Eq. (17), which is negative in the stable regime and becomes positive in the unstable regime.

the solution of the synchronization problem in one dimension. Generalizing to higher-dimensional systems will be straightforward.

We consider the equations of motion originating from the Hamiltonian in Eq.(7). We wish to integrate out the electron degrees of freedom and derive a closed-form dynamics for the oscillator. For that purpose we solve equations of motion for the i -th electron beginning from the time $t'_i < t$ when its state was last reset by scattering and the Hamiltonian dynamics described by Eq.(7) had started.

The equations of motion for the electrons and the oscillator are

$$\dot{p}_i = -\frac{\partial H}{\partial x_i} = eE + \alpha Q(t), \quad \dot{x}_i = \frac{\partial H}{\partial p_i} = \frac{\partial \epsilon(p_i)}{\partial p_i} \quad (8)$$

$$\dot{P} = -m\omega_0^2 Q + \sum_i \alpha x_i, \quad \dot{Q} = P/m. \quad (9)$$

Eliminating $P(t)$ yields the second-order equation of motion for the oscillator mode $Q(t)$, driven by an external force given by a sum of contributions due to the Bloch electrons

$$\ddot{Q}(t) + \omega_0^2 Q(t) = f(t), \quad f(t) = \frac{\alpha}{m} \sum_i x_i(t). \quad (10)$$

Importantly, the cumulative effect due to the Bloch electrons, given by the quantity $f(t)$, gives rise to a “memory effect” in the effective oscillator dynamics. Each term in the sum $\sum_i x_i(t)$ is given by a solution of the equations of motion for $x_i(t)$ and $p_i(t)$, Eq.(8), initialized at an earlier random time $t'_i < t$. The oscillator dynamics $Q(t)$,

$P(t)$ during the time intervals $t'_i < \tau < t$ affects the electron states $x_i(t)$, $p_i(t)$, giving rise to a back-action $f(t) = \frac{\alpha}{m} \sum_i x_i(t)$ with the dynamical memory originating from the dependence on $Q(\tau)$ and $P(\tau)$ at the earlier times $\tau < t$. As we show below, the feedback due to this memory effect enables synchronization of Bloch dynamics, resulting in a macroscopic oscillating current generated by Bloch-oscillating electrons. Here we average over the randomness in the starting times t'_i ignoring the associated noise. This simple approach will be sufficient to understand the synchronization effect. The role of randomness and noise will be discussed elsewhere.

To proceed, we will assume a simple band structure of the form

$$\epsilon(p) = -\Delta \cos\left(\frac{a}{\hbar}p\right),$$

where a is the lattice spacing. Integrating Bloch dynamics of the i -th electron for times $t'_i < \tau < t$ gives

$$p_i(t) = eE(t - t'_i) + \alpha \int_{t'_i}^t Q(\tau') d\tau' \quad (11)$$

$$x_i(t) = x_i(t'_i) + \int_{t'_i}^t v_0 \sin\left(\frac{a}{\hbar}p_i(\tau)\right) d\tau, \quad v_0 = \frac{a\Delta}{\hbar}.$$

Averaging over the starting times t'_i with the survival probability obeying the Poisson statistics $\gamma e^{-\gamma(t-t'_i)}$ gives

$$\langle x_i(t) \rangle = \langle x_i(t') \rangle + \int_{-\infty}^t dt' \gamma e^{-\gamma(t-t')} \int_{t'}^t d\tau v_0 \sin\left(\frac{a}{\hbar}p_i(\tau)\right)$$

$$= \int_{-\infty}^t dt' \gamma e^{-\gamma(t-t')} \int_{t'}^t d\tau v_0 \sin(\phi(\tau)), \quad (12)$$

where $\omega_B = eEa/\hbar$ is the Bloch frequency, and we denote $\phi(\tau) = \omega_B(\tau - t') + \frac{\alpha a}{\hbar} \int_{t'}^{\tau} Q(\tau') d\tau'$. Here we have dropped the starting displacement term $\langle x_i(t') \rangle$ assuming that it vanishes under averaging, as expected for a spatially uniform distribution.

The single mode dynamics is now described by Eq.(10) with the right-hand side replaced with a back-action memory function $\frac{\alpha}{m} N \langle x_i(t) \rangle$, where N is the number of Bloch electrons. We will consider the dynamics at lowest nonvanishing order in $Q(t)$, assuming the latter to be small. First, setting $Q(\tau') = 0$ and integrating over τ , we find $\langle x_i^{(0)}(t) \rangle = \frac{v_0 \omega_B}{\gamma^2 + \omega_B^2}$, a constant displacement that gives a time independent contribution to $f(t)$ in Eq.(10), which can be compensated for by shifting the oscillator equilibrium. Next, at first order in $Q(t)$, we Taylor-expand the sine term to obtain

$$\langle x_i^{(1)}(t) \rangle = \int_{-\infty}^t dt' \gamma e^{-\gamma(t-t')} \left(\int_{t'}^t d\tau v_0 \cos(\omega_B(\tau - t')) \left[\frac{\alpha a}{\hbar} \int_{t'}^{\tau} Q(\tau') d\tau' \right] \right). \quad (13)$$

Plugging in a harmonic dependence $Q(t) = Q_0 e^{-i\omega t}$, we evaluate the integrals over τ' and τ as

$$\begin{aligned} \int_{t'}^t d\tau v_0 \cos(\omega_B(\tau - t')) \left[\frac{\alpha a}{\hbar} \int_{t'}^{\tau} Q(\tau') d\tau' \right] &= \int_{t'}^t d\tau v_0 \cos(\omega_B(\tau - t')) \left[\frac{i\alpha a}{\hbar\omega} Q_0 (e^{-i\omega\tau} - e^{-i\omega t'}) \right] \\ &= \frac{i\alpha a v_0}{\hbar\omega} Q_0 \left(e^{-i\omega t} \frac{e^{i\omega_B(t-t')} - e^{i\omega(t-t')}}{i(\omega_B - \omega)} + e^{-i\omega t} \frac{e^{-i\omega_B(t-t')} - e^{i\omega(t-t')}}{-i(\omega_B + \omega)} - e^{-i\omega t'} \frac{\sin \omega_B(t-t')}{\omega_B} \right). \end{aligned} \quad (14)$$

Integration over $t' < t$ in Eq.(13) can now be carried out with the help of the identity

$$\int_{-\infty}^t dt' \gamma e^{-\gamma(t-t')} e^{-i\Omega(t-t')} = \frac{\gamma}{\gamma + i\Omega},$$

giving

$$\begin{aligned} \langle x_i^{(1)}(t) \rangle &= \frac{i\alpha a v_0}{\hbar\omega} Q_0 e^{-i\omega t} \left(\frac{\frac{\gamma}{\gamma - i\omega_B} - \frac{\gamma}{\gamma - i\omega}}{i(\omega_B - \omega)} + \frac{\frac{\gamma}{\gamma + i\omega_B} - \frac{\gamma}{\gamma - i\omega}}{-i(\omega_B + \omega)} - \frac{\frac{\gamma}{\gamma - i(\omega + \omega_B)} - \frac{\gamma}{\gamma - i(\omega - \omega_B)}}{2i\omega_B} \right) \\ &= \frac{i\alpha a v_0}{\hbar\omega} Q_0 e^{-i\omega t} \left(\frac{\gamma}{(\gamma - i\omega_B)(\gamma - i\omega)} + \frac{\gamma}{(\gamma + i\omega_B)(\gamma - i\omega)} - \frac{\gamma}{(\gamma - i(\omega + \omega_B))(\gamma - i(\omega - \omega_B))} \right) \\ &= \frac{i\alpha a v_0}{\hbar\omega} Q_0 e^{-i\omega t} \left(\frac{2\gamma^2}{(\gamma^2 + \omega_B^2)(\gamma - i\omega)} + \frac{\gamma}{(\omega + i\gamma)^2 - \omega_B^2} \right). \end{aligned} \quad (15)$$

Substituting this result in Eq.(10) gives a characteristic equation for ω of the form

$$\begin{aligned} \omega_0^2 - \omega^2 &= \frac{i\lambda}{\omega} \left(\frac{2\gamma^2}{(\gamma^2 + \omega_B^2)(\gamma - i\omega)} + \frac{\gamma}{(\omega + i\gamma)^2 - \omega_B^2} \right), \\ \lambda &= N \frac{\alpha^2 a v_0}{m\hbar} = N \left(\frac{\alpha a}{\hbar} \right)^2 \frac{\Delta}{m}, \end{aligned} \quad (16)$$

where N is the total number of Bloch-oscillating electrons.

The system becomes unstable when Eq.(16) admits solutions in the upper halfplane of complex ω . Before exploring this instability we inspect, as a sanity check, the regime of highly damped Bloch oscillations, $\gamma \gg \omega_B, \omega_0$. In this case, Eq.(16) reads $\omega_0^2 - \omega^2 = \frac{i\lambda}{\omega\gamma}$. At large γ , the roots of this equation are close to $\pm\omega_0$. Writing $\omega = \pm\omega_0 + \Delta\omega$, at leading order in $1/\gamma$ we find $\Delta\omega = -i\frac{\lambda}{\omega_0^2\gamma}$. Negative imaginary part indicates that no instability arises in this regime, i.e. the driven system is stabilized by high damping.

Next, we consider a weak damping $\gamma \ll \omega_B, \omega_0$. The behavior in this case is simplest to understand close to the resonance between the oscillator and Bloch frequencies, $\omega_0 \approx \omega_B$. Focusing on the frequencies ω near the resonance, where the last term in Eq.(16) dominates, we ignore the first non-resonant term and obtain

$$(\omega_0^2 - (\omega + i\gamma_0)^2)((\omega + i\gamma)^2 - \omega_B^2) = \frac{i\lambda\gamma}{\omega}. \quad (17)$$

Here we added the damping rate γ_0 for the oscillator. Working near the resonance and expanding in a small $\delta\omega = \omega - \omega_0 \ll \omega_0 \approx \omega_B$ to obtain the complex frequency roots positioned near ω_0 , the characteristic equation becomes

$$(\omega - \omega_0 + i\gamma_0)(\omega + i\gamma - \omega_B) = -i\eta/4, \quad \eta = \frac{\lambda\gamma}{\omega_0^3}. \quad (18)$$

The properties of Eq.(18) are simplest to understand when $\gamma_0 = \gamma$. In this case, the roots are

$$\omega_{1,2} = -i\gamma + \frac{\omega_B + \omega_0 \pm \sqrt{(\omega_B - \omega_0)^2 - i\eta}}{2} \quad (19)$$

The system is stable if $\text{Im} \omega_{1,2} < 0$ and unstable otherwise. Using the identity

$$\text{Im} \left(\sqrt{x - i\eta} \right) = -\text{sgn} \eta \sqrt{\frac{\sqrt{x^2 + \eta^2} - x}{2}} \quad (20)$$

with $x = (\omega_B - \omega_0)^2$, we can write the condition for the instability as

$$\eta^2 > \left((\omega_B - \omega_0)^2 + 4\gamma^2 \right) 16\gamma^2. \quad (21)$$

This criterion predicts the Bloch frequency ω_B and the coupling strength λ values for which an instability may

occur, giving the phase diagram pictured in Fig.3. As one might expect on general grounds, the instability is easiest to achieve when Bloch oscillations are in resonance with the oscillator, $\omega_B = \omega_0$. Tuning away from the resonance suppresses the instability. The instability signals the onset of a collective regime in which Bloch-oscillating electrons become synchronized through coupling to the oscillator mode.

It is instructive to extend this analysis to the more general case of unequal damping rates for the oscillator and electrons, $\gamma_0 \neq \gamma$. After some algebra we arrive at the instability criterion

$$(\eta + 2(\gamma - \gamma_0)(\omega_B - \omega_0))^2 > ((\omega_B - \omega_0)^2 + 4\gamma\gamma_0) \times 4(\gamma + \gamma_0)^2. \quad (22)$$

A new interesting behavior found for $\gamma_0 \neq \gamma$ is an asymmetry between ω_B blue-shifted and red-shifted away from ω_0 , with the instability threshold lower for $\omega_B > \omega_0$ and higher for $\omega_B < \omega_0$ when $\gamma_0 < \gamma$, and vice versa when $\gamma_0 > \gamma$. The asymmetry is particularly striking in the limit $\gamma_0/\gamma \rightarrow 0$: for $\omega_B > \omega_0$ the instability occurs at the coupling values η much smaller than those in Eq.(21), whereas for $\omega_B < \omega_0$ the instability threshold remains on the same order as in Eq.(21). Furthermore, perhaps somewhat counterintuitively, for $\gamma_0/\gamma \rightarrow 0$ the lowest value of coupling at which the instability sets in occurs far away from the resonance $\omega_B = \omega_0$.

The origin of this asymmetry is closely related to the mechanism that enables the synchronized behavior. When the oscillator is undamped, synchronization arises due to the electrons pumping energy into the oscillator mode; subsequently, when this energy is passed back to electrons, they become synchronized with the oscillator, and with each other. However, at a weak coupling η , the energy transfer from the Bloch-oscillating electrons into the oscillator is possible only if $\hbar\omega_B > \hbar\omega_0$, indicating that the instability is easier to reach for ω_B values blue-shifted from ω_0 .

The above argument also suggests a reversal in the asymmetry when Bloch oscillations are weakly damped

compared to the oscillator damping, $\gamma \ll \gamma_0$. Indeed, in this case it is the electron subsystem that serves as the main reservoir for energy storage, whereas the role of the oscillator mode is merely to lock the phases of different Bloch oscillating carriers. Pumping energy into the collective mode now requires $\hbar\omega_B < \hbar\omega_0$. We therefore expect that in this limit the instability will occur at lower η values for ω_B red-shifted from ω_0 , which is exactly what Eq.(22) predicts.

In summary, previous efforts to achieve collective Bloch oscillations in superlattice arrays of stacked semiconductor quantum wells came tantalizingly close to achieving this regime, however encountered obstacles due to electric field instabilities and noise. Here we propose a new system, the flat bands in moiré graphene, and argue that their unique electronic properties, such as the bandwidth considerably narrower than the Debye energy scale, the $\sim 10\text{nm}$ -large superlattice periodicity and relatively high mobility, will facilitate observing the Bloch oscillations. Since carriers in two-dimensional systems are fully exposed, they can be coupled to a nearby oscillator mode that will synchronize movements of different carriers and enable achieving phase-coherent oscillations. A detailed analysis of the free-carrier Bloch oscillations synchronized by introducing an oscillator mode coupled to carrier displacements indicates feasibility of moiré-graphene-based Bloch oscillators. The instability achieved near the resonance between the Bloch frequency and the oscillator frequency is followed by a transition from asynchronous Bloch oscillations of free carriers to the synchronized collective-oscillation regime. The synchronized phase-coherent Bloch dynamics, driven by a DC current, has a potential to provide electromagnetic radiation sources with a stable and tunable frequency, realized at the submicron scale. The two-dimensional geometry of the moiré graphene systems is beneficial for overcoming the electric field domain formation encountered in previous work. The narrow bands in moiré superlattices therefore offer a unique platform in which Bloch oscillators driven by a DC current can be realized and explored.

-
- [1] N. W. Ashcroft and N. D. Mermin, *Solid State Physics* (Saunders, Philadelphia, 1976).
 - [2] A. B. Pippard, *The Dynamics of Conduction Electrons* (Gordon and Breach Science Publishers, Inc., New York, 1965).
 - [3] L. Esaki and R. Tsu, *Superlattice and Negative Differential Conductivity in Semiconductors*, IBM J. Res. Dev., **14**, 61-65 (1970).
 - [4] S. A. Kitorov, G. S. Simin, and V. Y. Sindalovskii, Bragg reflections and the high-frequency conductivity of an electronic solid-state plasma, *Fizika Tverdogo Tela*, **13**, 2230-2233 (1971) [*Soviet Physics - Solid State* **13**, 1872-1874 (1972)]
 - [5] H. Kroemer, On the nature of the negative-conductivity resonance in a superlattice Bloch oscillator, arXiv:cond-mat/0007482 (2000).
 - [6] P. G. Savvidis, B. Kolasa, G. Lee, and S. J. Allen, Resonant Crossover of Terahertz Loss to the Gain of a Bloch Oscillating InAs/AlSb Superlattice, *Phys. Rev. Lett.* **92**, 196802 (2004).
 - [7] A. Sibille, J. F. Palmier, H. Wang, and F. Mollot, Observation of Esaki-Tsu negative differential velocity in GaAs/AlAs superlattices, *Phys. Rev. Lett.* **64**, 52 (1990).
 - [8] J. Feldmann, K. Leo, J. Shah, D. A. B. Miller, and J. E. Cunningham, T. Meier, G. von Plessen, A. Schulze, P. Thomas, and S. Schmitt-Rink, Optical investigation of Bloch oscillations in a semiconductor superlattice, *Phys. Rev. B* **46**, 7252 (1992).

- [9] C. Waschke, H. G. Roskos, R. Schwedler, K. Leo, H. Kurz, and K. Kohler, Coherent submillimeter-wave emission from Bloch oscillations in a semiconductor superlattice, *Phys. Rev. Lett.* **70**, 3319 (1993).
- [10] A. Rauh and G. H. Wannier, Theory of stark ladders in the optical absorption of solids, *Solid State Commun.* **15**, 1239 (1974).
- [11] T. Hyart, K. N. Alekseev, and E. V. Thuneberg, Bloch gain in dc-ac-driven semiconductor superlattices in the absence of electric domains, *Phys. Rev. B* **77**, 165330 (2008).
- [12] T. Hyart, N. V. Alexeeva, J. Mattas, and K. N. Alekseev, Terahertz Bloch Oscillator with a Modulated Bias, *Phys. Rev. Lett.* **102**, 140405 (2009).
- [13] T. Hyart, J. Mattas, and K. N. Alekseev, Model of the Influence of an External Magnetic Field on the Gain of Terahertz Radiation from Semiconductor Superlattices, *Phys. Rev. Lett.* **103**, 117401 (2009).
- [14] M. Ben Dahan, E. Peik, J. Reichel, Y. Castin, and C. Salomon, Bloch Oscillations of Atoms in an Optical Potential, *Phys. Rev. Lett.* **76**, 4508 (1996).
- [15] B. P. Anderson, M. A. Kasevich, Macroscopic Quantum Interference from Atomic Tunnel Arrays, *Science* **282** (5394), 1686-1689 (1998).
- [16] O. Morsch, J. H. Muller, M. Cristiani, D. Ciampini, and E. Arimondo, Bloch Oscillations and Mean-Field Effects of Bose-Einstein Condensates in 1D Optical Lattices, *Phys. Rev. Lett.* **87**, 140402 (2001).
- [17] M. Cristiani, O. Morsch, J. H. Muller, D. Ciampini, and E. Arimondo, Experimental properties of Bose-Einstein condensates in one-dimensional optical lattices: Bloch oscillations, Landau-Zener tunneling, and mean-field effects, *Phys. Rev. A* **65**, 063612 (2002).
- [18] H. Ott, E. de Mirandes, F. Ferlaino, G. Roati, G. Modugno, and M. Inguscio, Collisionally Induced Transport in Periodic Potentials, *Phys. Rev. Lett.* **92**, 160601 (2004).
- [19] M. Gluck, F. Keck, A. R. Kolovsky, and H. J. Korsch, Wannier-Stark resonances in optical and semiconductor superlattices, *Phys. Reps.* **366** (3), 103-182 (2002).
- [20] I. A. Dmitriev and R. A. Suris *Semiconductors* **35**, 212 (2001).
- [21] I. A. Dmitriev and R. A. Suris *Semiconductors* **36**, 1364 (2002).
- [22] A. R. Kolovsky, E. N. Bulgakov, Wannier-Stark states and Bloch oscillations in the honeycomb lattice, *Phys. Rev. A* **87** (3), 033602 (2013).
- [23] R. Bistritzer and A. H. MacDonald, Moiré bands in twisted double-layer graphene. *Proc. Nat. Acad. Sci.* **108**, 12233-12237 (2011).
- [24] Y. Cao, V. Fatemi, A. Demir, S. Fang, S. L. Tomarken, J. Y. Luo, J. D. Sanchez-Yamagishi, K. Watanabe, T. Taniguchi, E. Kaxiras, R. C. Ashoori, and P. Jarillo-Herrero, Correlated insulator behaviour at half-filling in magic-angle graphene superlattices. *Nature* **556**, 80-84 (2018).
- [25] Y. Cao, V. Fatemi, S. Fang, K. Watanabe, T. Taniguchi, E. Kaxiras, and P. Jarillo-Herrero, Unconventional superconductivity in magic-angle graphene superlattices. *Nature* **556**, 43-50 (2018).
- [26] Y. Cao, J. Y. Luo, V. Fatemi, S. Fang, J. D. Sanchez-Yamagishi, K. Watanabe, T. Taniguchi, E. Kaxiras, and P. Jarillo-Herrero, Superlattice-Induced Insulating States and Valley-Protected Orbits in Twisted Bilayer Graphene. *Phys. Rev. Lett.* **117**, 116804 (2016).
- [27] Y. Kim, P. Herlinger, P. Moon, M. Koshino, T. Taniguchi, K. Watanabe and J. H. Smet, Charge Inversion and Topological Phase Transition at a Twist Angle Induced van Hove Singularity of Bilayer Graphene, *Nano Lett.* **16**, 5053-5059 (2016).
- [28] A. I. Berdyugin, B. Tsim, P. Kumaravadivel, S. G. Xu, A. Ceferino, A. Knothe, R. Krishna Kumar, T. Taniguchi, K. Watanabe, A. K. Geim, I. V. Grigorieva, V. I. Fal'ko, Minibands in twisted bilayer graphene probed by magnetic focusing, *Sci. Adv.* **6**: eaay7838 (2020)
- [29] R. Bistritzer and A. H. MacDonald, Electronic cooling in graphene, *Phys. Rev. Lett.*, **102**, 206410 (2009).
- [30] W. K. Tse, S. Das Sarma, Energy relaxation of hot Dirac fermions in graphene. *Phys. Rev. B* **79**, 235406 (2009).
- [31] J. C. W. Song, M. Y. Reizer, L. S. Levitov, Disorder-assisted electron-phonon scattering and cooling pathways in graphene. *Phys. Rev. Lett.* **109**, 106602 (2012).
- [32] L. Ju, et al. Graphene plasmonics for tunable terahertz metamaterials. *Nat. Nanotechnol.* **6**, 630-643 (2011).
- [33] H. Yan, et al. Tunable infrared plasmonic devices using graphene/insulator stacks. *Nat. Nanotechnol.* **7**, 330-334 (2012).
- [34] H. Yan, et al. Infrared spectroscopy of tunable dirac terahertz magneto-plasmons in graphene. *Nano. Lett.* **12**, 3766-3771 (2012).
- [35] N. H. Tu, K. Yoshioka, S. Sasaki, M. Takamura, K. Muraki and N. Kumada, Active spatial control of terahertz plasmons in graphene, *Communications Materials* volume 1, Article number: 7 (2020)
- [36] L. Ateshian, H. Choi, M. Heuck, and D. Englund, Terahertz Light Sources by Electronic-Oscillator-Driven Second Harmonic Generation in Extreme-Confinement Cavities, arXiv:2009.13029
- [37] Sh. M. Kogan and A. Ya. Shulman, Extraneous random forces and equations for correlation functions in the theory of nonequilibrium fluctuations, *Fiz. Tverd. Tela (Leningrad)* **12**(4), 1119-1123 (1970) [*Sov. Phys. – Solid State* **12**(4), 874 (1970)].
- [38] Sh. Kogan, *Electronic Noise and Fluctuations in Solids* (Cambridge University Press, 2008)